Journal of Power Sources 186 (2009) 377–384

Contents lists available at ScienceDirect

Journal of Power Sources

journal homepage: www.elsevier.com/locate/jpowsour

Thermodynamic analysis of solid oxide fuel cells operated with methanol and ethanol under direct utilization, steam reforming, dry reforming or partial oxidation conditions

M. Cimenti, J.M. Hill*

Department of Chemical and Petroleum Engineering, University of Calgary, Calgary, 2500 University Dr. NW, Canada

ARTICLE INFO

Article history:
Received 21 August 2008
Received in revised form 10 October 2008
Accepted 10 October 2008
Available online 21 October 2008

Keywords:
Solid oxide fuel cells
Direct utilization
Partial oxidation
Methanol
Ethanol
Carbon deposition boundary

ABSTRACT

There is increasing interest in developing solid oxide fuel cells (SOFC) for portable applications. For these devices it would be convenient to directly use a liquid fuel such as methanol and ethanol rather than hydrogen. The direct utilization of alcohol fuels in SOFC involves several processes, including the deposition of carbon, which can lead to irreversible deactivation of the fuel cell. Several publications have addressed the thermodynamic analysis of the reforming of methanol (MeOH) and ethanol (EtOH) in SOFC, but none have considered the direct utilization of these fuels. The equilibrium compositions, the carbon deposition boundaries, and the electromotive forces for the direct utilization and partial oxidation of methanol and ethanol in SOFC as a function of the fuel utilization are obtained in this study. In addition, the minimum amounts of H_2O, and CO_2 for direct and indirect reforming with MeOH and EtOH to avoid carbon formation are calculated.

1. Introduction

Fuel cells are currently considered as the most efficient and clean alternative to convert the chemical energy of a fuel into electricity, and extensive research is ongoing to improve the reliability and reduce the cost of these electrochemical devices [1]. Most fuel cell types require hydrogen as fuel [1], but hydrogen is expensive and difficult to store if compared to traditional hydrocarbon fuels. Thus, there is an increasing interest in developing fuel cells that also operate with traditional fuels, such as natural gas, propane, gasoline, and diesel. Among all types, solid oxide fuel cells (SOFC) offer better fuel versatility; in fact, synthesis gas is typically used to fuel SOFC by integrating a fuel-reforming unit within the system [2]. There also have been several reports on SOFC operating with partial oxidation of conventional fuels (e.g. propane [3]) and with the direct utilization of natural gas and other hydrocarbons [4,5]. However, the utilization of synthesis gas and, in particular, the direct utilization of hydrocarbons can lead to rapid deactivation by sulfur poisoning and/or carbon formation on the traditional SOFC anode [2] (i.e. a composite of nickel and yttria-stabilized zirconia, Ni/YSZ). In the case of direct utilization, carbon formation can be particularly severe, causing the delamination of the Ni/YSZ anode [6] that rapidly and irreversibly destroys the cell.

Although SOFC are intended mainly for medium-large stationary applications, where a reforming unit can be easily integrated, there is an increasing interest in developing SOFC for portable applications, such as portable power generation units and auxiliary power units in military and transportation uses [7]. For these applications, it would be ideal to use a liquid fuel, which is easy to store and transport, and to operate the cell in the direct utilization or partial oxidation modes, which allows a reduction of the size, complexity, and cost of the system [2]. Methanol (MeOH) and ethanol (EtOH) have recently received much attention as liquid fuels particularly as alternative 'energy-vectors' for the future [8]. Both of these fuels have a very low content of impurities (<0.2%), are oxygenated, which drastically reduces the risks of sulfur-poisoning and carbon formation, and are candidate fuels for portable SOFC applications.

The direct utilization of alcohols in SOFC involves many reaction processes in both the gas phase and at the anode, including: (1) pyrolysis in the gas-channels, (2) catalytic decomposition on the anode surface, (3) electrochemical oxidation in proximity of the triple-phase boundary, (4) steam and dry reforming on the anode surface and/or oxidation of the fuel, (5) water–gas shift reaction on the anode surface, and (6) carbon deposition and removal.

* Corresponding author. Tel.: +1 403 2109488.
E-mail addresses: max.cimenti@afcc-auto.com (M. Cimenti), jhill@ucalgary.ca (J.M. Hill).

0378-7753/$ – see front matter © 2008 Elsevier B.V. All rights reserved.
doi:10.1016/j.jpowsour.2008.10.043

Nomenclature

CDB	carbon deposition boundary
E^0	equilibrium potential
EMF	electromotive force
ES_{i-j}	equilibrium selectivity for species *i* and *j*
EtOH	ethanol
Ey_i	equilibrium yield for species *i*
F	Faraday constant (96485.34 C mol^{-1})
MeOH	methanol
$n_{fuel\text{-}in}$	molar flow rate of alcohol fuel at the inlet
$n_{fuel\text{-}eq}$	molar flow rate of alcohol fuel at the outlet at equilibrium
$n_{i\text{-}eq}$	molar flow rate of species *i* at the outlet at equilibrium
$n_{O_2\text{-}echem}$	molar flow rate of oxygen due to electrochemical oxidation
$n_{O_2\text{-}leak}$	molar flow rate of oxygen due to air leaks
n_{O_2-POX}	molar flow rate of oxygen due to POX
OCP	open circuit potential
POX	partial oxidation
RF_{H_2O}	steam-reforming factor
RF_{CO_2}	dry-reforming factor
SOFC	solid oxide fuel cell
U_f	fuel utilization
$U_{f\text{-}app}$	apparent fuel utilization
X_{max}	maximum fuel conversion
z	number of electrons produced per alcohol molecule

The extent of each reaction is related to the flow conditions, temperature gradients, and overall current. Carbon deposition, which can deactivate and/or mechanically destroy the anode, will happen whenever there is a positive driving force for the deposition reactions. According to the affinity concept (see [9]), this driving force is in the first approximation proportional to the difference between the actual and the equilibrium activities for the reacting species.

Typically the SOFC operating conditions (e.g. steam to carbon ratio) are chosen to completely avoid carbon formation. Although SOFC may not operate at equilibrium, thermodynamic analysis of gas-phase compositions and carbon formation provides a useful guideline. Several studies on the equilibrium for dry and steam reforming have been reported [10–14], and few studies on the internal reforming and partial oxidation of methanol and ethanol [15,16]. The focus of these publications was on the identification of the minimum H_2O, CO_2 and air requirements to prevent carbon deposition for external or internal reforming of several hydrocarbon fuels, but no attention was given to the variations of the equilibrium conditions with the degree of oxidation of the fuel. Only one study addressed the variation of the carbon deposition boundaries as a function of the current density for the direct utilization of methane in SOFC [17]. Cairns et al. [18,19] provided a general treatment of the equilibrium for low temperature (<500 K) hydrocarbon fuel cells. In fact, understanding the variations of equilibrium composition and electromotive force (EMF) as a function of the fuel utilization is fundamentally important for an SOFC operating in the direct utilization and partial oxidation modes. Thus, the work of Cairns et al. [18,19] was used as a guide for the study herein.

The objective of the work reported in this paper is to obtain equilibrium compositions, carbon deposition boundaries, and electromotive forces for the direct utilization and partial oxidation of MeOH and EtOH in SOFC. To reach this objective the pyrolysis, steam-reforming, and dry-reforming conditions were studied with and without the presence of a current. The minimum amounts of H_2O, CO_2 and O_2 to avoid carbon deposition for SOFC fuelled directly or indirectly with MeOH and EtOH are also reported. All values were obtained using a nonstoichiometric formulation approach and calculations were performed with the software Chemical Equilibrium with Applications (CEA) developed by NASA.

2. Theory and calculations

Equilibrium compositions at the anode of an SOFC were calculated by assuming perfectly mixed isothermal reactor conditions for the anodic compartment (i.e. homogeneous temperature and pressure) with fuel-gas fed at a constant rate. The amounts of each species present at equilibrium in the gaseous and solid phases were obtained in the temperature range between 773 and 1173 K, at intervals of 25 K, and for a total pressure of 1 bar. The type of carbon that forms at an anode is complex and depends on many factors [20]. For the majority of the present calculations, graphite was considered as the only allotropic species for solid carbon present at equilibrium. Some calculations were performed to assess the implications of including amorphous carbon, rather than graphite, in the equilibrium calculations.

At constant temperature and pressure the Gibbs free energy for a system at equilibrium is at a global minimum. The basic criterion for the establishment of chemical equilibrium is given by:

$$(dG_{SYS})_{T,p} = 0 \quad (1)$$

This criterion was used for the determination of the equilibrium compositions in the anodic compartment. There are two different approaches to solve this problem. The first, called stoichiometric formulation [21], essentially requires the solution of a system of nonlinear equations obtained using the stoichiometric equations of the chemical reactions considered to obtain the minimum of Eq. (1). The second approach, called nonstoichiometric formulation, minimizes the Gibbs free energy as a function of the moles of a large collection of species using, for example, the method of Lagrange multipliers, and does not require the assumption of any chemical reactions. The solutions obtained using the two procedures are equivalent, provided that a complete set of reactions is used in the first approach [21]. The equilibrium compositions presented in this study were calculated numerically using the software CEA (Chemical Equilibrium with Applications) developed by NASA.[1] CEA implements the nonstoichiometric formulation, and uses a database of thermodynamic properties containing over 2000 species, including solids, liquids and gases. The results obtained using CEA for a few basic cases and the implications of considering amorphous carbon rather than graphite were verified using the commercial software for thermodynamic calculations FactSage 5.4,[2] which also utilizes a nonstoichiometric method. In all cases checked, the equilibrium results obtained by CEA and FactSage were essentially identical.

The equilibrium compositions plotted in this work are expressed as maximal fractional conversion, equilibrium yield and selectivity according to the following definitions [22]:

$$X_{max} = \frac{n_{fuel\text{-}in} - n_{fuel\text{-}eq}}{n_{fuel\text{-}in}} \quad (2)$$

$$Ey_i = \frac{n_{i\text{-}eq}}{n_{fuel\text{-}in} - n_{fuel\text{-}eq}} \quad (3)$$

$$ES_{i-j} = \frac{n_{i-eq}}{n_{j-eq}} \quad (4)$$

[1] www.grc.nasa.gov/WWW/CEAWeb/.
[2] www.factsage.com.

where X_{max} is the fuel conversion at equilibrium, Ey_i is the equilibrium yield for species i, ES_{i-j} is the equilibrium selectivity for species i relative to species j, $n_{fuel\text{-}in}$ and $n_{fuel\text{-}eq}$ are the initial and equilibrium molar flow rates, respectively, of the fuel and $n_{i\text{-}eq}$ is the equilibrium molar flow rate for species i.

When an SOFC is producing a current there is a net input of oxygen ions (O^{2-}) to the anodic compartment that changes the equilibrium conditions and so calculations were performed for various current loads. In the case of direct utilization, the new equilibrium composition can be predicted considering that the oxygen inflow due to electrochemical oxidation is related to the fuel utilization by Eq. (5):

$$n_{O_2\text{-}echem} = 0.25\, z\, U_f\, n_{fuel\text{-}in} \quad (5)$$

where z is the number of electrons produced by the oxidation of 1 alcohol molecule (i.e. 6 electrons for MeOH and 12 electrons for EtOH), $n_{O_2-echem}$ is the molar flow rate of oxygen, and U_f is the fuel utilization. The fuel utilization (U_f) is related to the overall current produced by the cell (I_{TOT}) by:

$$I_{TOT} = zFU_f n_{fuel-in} \quad (6)$$

where F is the Faraday constant. In the case of partial oxidation, there is an additional input of O_2. Similarly, the presence of air leaks further increases the O_2 inflow, while the presence of N_2 dilutes the feed. The total oxygen input to the anodic compartment is given by the sum of these inflows, and the apparent fuel utilization is given by:

$$U_{f\text{-}app} = U_f + \frac{n_{O_2\text{-}POX} + n_{O_2\text{-}leak}}{0.25 z n_{fuel\text{-}in}} \quad (7)$$

where n_{O_2-POX} and n_{O_2-leak} are the moles of oxygen admitted with the fuel (in the case of POX) and through any leaks, respectively. In this study, the equilibrium compositions were calculated as a function of the fuel utilization for mixtures of alcohol–fuel and O_2 according the ratio given by Eq. (5).

The carbon deposition boundaries (CDB) were obtained by calculating the equilibrium composition over a range of alcohol–fuel to H_2O, CO_2, or O_2 ratios. The carbon formation region is identified by the conditions for which the amount of graphite present at equilibrium is larger than 1E−6 mole fractions. Likewise, the carbon free region corresponds to conditions for which graphite at equilibrium is smaller than 1E−6 mole fractions.

The electromotive force was calculated using the Nernst equation including all species present at equilibrium (including graphite) at the anode, and only air at the cathode ($pO_2 = 0.206 P_{TOT}$). The heat capacities, enthalpies and entropies of formation used were those tabulated by the database DIPPR [23]. The activity for graphite was assumed equal to unity, while the fugacity of the gaseous species was assumed equivalent to the equilibrium partial pressures.

In a real cell, the maximum fuel utilization that can be reached for a given fuel flow rate depends on the actual cell performance (i.e. i–V curve) according to Eq. (8):

$$U_{f\text{-}max} = \frac{I_{lim}}{zFn_{fuel\text{-}in}} \quad (8)$$

where I_{lim} is the limiting or the maximum current for the cell. The maximum current achievable with the SOFC depends on several factors, e.g. ohmic and mass transfer limitations, electrochemical overpotential of anode and cathode. Eqs. (7) and (8) can be used to verify whether an experimental SOFC is operating outside the carbon formation region during experiments of direct utilization with alcohols.

3. Results and discussion

3.1. Equilibrium compositions with methanol feed

The equilibrium composition for the pyrolysis of MeOH as a function of temperature is shown in Fig. 1. In all figures, the symbols represent points at which calculations were performed, while the lines represent the trend. The only species present at equilibrium are hydrogen (H_2), carbon monoxide (CO), methane (CH_4), carbon dioxide (CO_2), water (H_2O) and graphite (C). The equilibrium conversion of MeOH is 100% at all temperatures (i.e. MeOH is entirely decomposed). The presence of C is predicted over the entire temperature range. The equilibrium concentration of C decreases with temperature, from 16.6 mol% at 773 K to only 0.2 mol% at 1173 K. Within the operational conditions typical of SOFC, i.e. 973–1073 K, the concentration of C changes from 7.5 to 1.9 mol%, respectively, indicating that the 'driving force' for the carbon deposition reaction decreases with temperature. In practice, carbon deposition may be highly dependent on kinetics.

As shown in Fig. 1b, the gas-phase is composed mostly by H_2 (approximately 62 vol%) and CO (approximately 25 vol%). CH_4, CO_2 and H_2O become less prevalent at higher temperatures. The H_2 to CO ratio (H_2/CO) approaches 2 with increasing temperature. At 1073 K the H_2/CO is 2.1, indicating that the direct decomposition to H_2 and CO (i.e. $CH_3OH = 2H_2 + CO$) is the predominant reaction (i.e. most negative Gibbs free energy change and largest equilibrium constant) among all the possible reactions involving MeOH. This result can be verified by applying the stoichiometric method for the decomposition reaction. As a result, the gas-phase com-

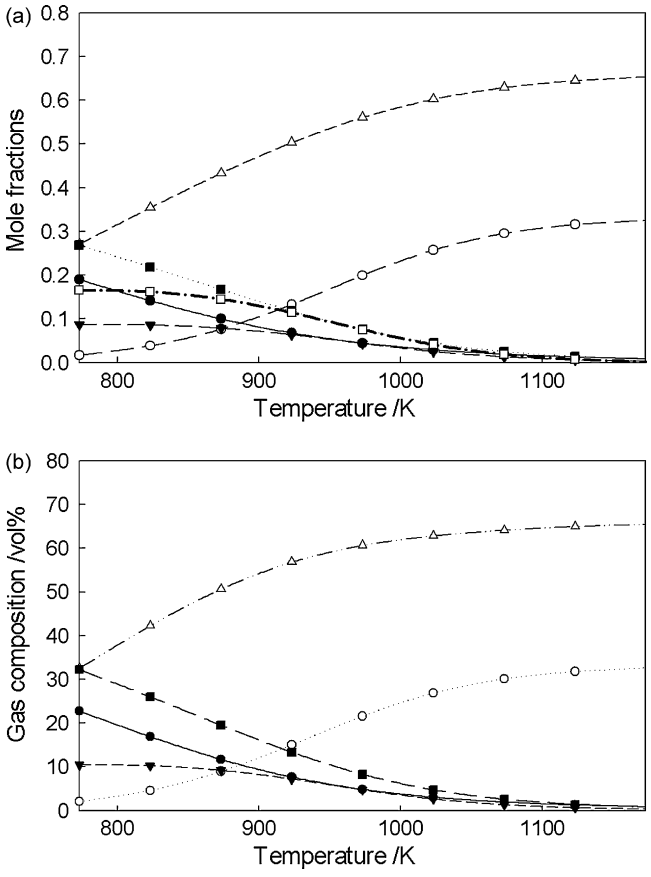

Fig. 1. Equilibrium composition (a) and gas-phase concentrations (b) as a function of temperature for the reaction of MeOH pyrolysis. The species at equilibrium are (●) CH_4, (○) CO, (▼) CO_2, (□) H_2, (■) H_2O, and (□) C (graphite).

Table 1
Minimum reforming factors required to avoid carbon formation in the steam- and dry-reforming of methanol, and the resulting H_2 yield, CH_4 yield and H_2/CO ratios.

T (K)	MeOH steam-reforming				MeOH dry-reforming			
	RF_{H_2O}	Ey_{H_2}	Ey_{CH_4}	$ES_{H_2/CO}$	RF_{CO_2}	Ey_{H_2}	Ey_{CH_4}	$ES_{H_2/CO}$
773	0.848	0.827	0.526	12.186	38.000	0.503	0.013	0.206
823	0.828	1.153	0.422	7.180	14.500	0.720	0.028	0.332
873	0.704	1.446	0.309	4.559	5.500	0.973	0.050	0.533
923	0.499	1.650	0.209	3.197	1.900	1.252	0.078	0.872
973	0.288	1.762	0.134	2.514	0.614	1.511	0.087	1.322
1023	0.140	1.827	0.086	2.200	0.205	1.700	0.072	1.681
1073	0.060	1.873	0.056	2.070	0.072	1.817	0.052	1.865
1123	0.023	1.908	0.037	2.020	0.025	1.887	0.036	1.946
1173	0.007	1.934	0.025	2.002	0.007	1.927	0.025	1.981

position in this case, can be well estimated by only considering the MeOH decomposition reaction. Species such as formaldehyde (HCHO) and ethylene (C_2H_4) are not found at equilibrium because they are unstable relative to CH_4, CO, and CO_2. In fact, HCHO is an important intermediate of decomposition and is found when the pyrolysis of MeOH is not complete [24]. The results shown in Fig. 1 are representative of the equilibrium state in the anode compartment of a SOFC at OCP (i.e. zero current) when the fuel consists of pure methanol.

Equilibrium calculations were performed to identify the conditions at which carbon deposition can be avoided for steam and dry reforming of MeOH; the results are summarized in Table 1. The steam-reforming factor (RF_{H_2O}) and dry-reforming factor (RF_{CO_2}) are defined as the molar ratios of H_2O to MeOH and CO_2 to MeOH, respectively, required to prevent carbon (as graphite) deposition. The equilibrium compositions for the given reforming factors are reported in terms of equilibrium yields (Ey_{H_2}, Ey_{CH_4}) and selectivities ($ES_{H_2/CO}$, ES_{H_2/CH_4}) as defined in Eqs. (3) and (4). Note that the equilibrium conversion for both steam and dry reforming is 100% over the entire temperature range.

For the steam-reforming of MeOH the minimum value of the reforming factor that should be used to avoid carbon formation is 0.060 at 1073 K (i.e. 6 mol of H_2O per 100 mol of MeOH). Considering that dry MeOH is hygroscopic, it is evident that the use of highly pure feedstock is paramount if the direct utilization of this fuel is to be studied. In fact, if the liquid MeOH feedstock used to fuel a SOFC at 1073 K contains more than 2.6 vol% of H_2O, the mode of operation is direct internal reforming rather than direct utilization. The reforming factor decreases with temperature, in accordance with the results previously shown for MeOH pyrolysis (Fig. 1). Considering the equilibrium compositions corresponding to the minimum reforming factors, for temperatures higher than 1073 K, $ES_{H_2/CO}$ is approximately 2, indicating that MeOH has formed almost exclusively H_2 and CO.

At temperatures lower than 923 K, the dry-reforming of MeOH requires high ratios of CO_2 to MeOH (between 1.9 and 38) to avoid carbon formation. At 773 K, an equimolar mixture of MeOH and CO_2 produces 20 mol% more carbon at equilibrium than MeOH pyrolysis. Conversely, at temperatures greater than 1073 K both Ey_{H_2} and $ES_{H_2/CO}$ approach 2, indicating that MeOH has essentially only formed H_2 and CO, similar to the result for steam-reforming of MeOH.

The equilibrium compositions were calculated as a function of the fuel utilization considering an inlet stream composed of dry MeOH with oxygen from the cathode in the proportions given by Eq. (5). The region of carbon deposition shown in Fig. 2a is identified by the minimum fuel utilization for which graphite is absent (<1E−6 mole fraction) from the equilibrium mixture at a given temperature. The CDB shifts towards lower fuel utilization as the temperature increases. The CDB as a function of the fuel utilization shown in Fig. 2a also can be used to determine the minimum amount of air required to avoid coke formation for the partial oxidation of methanol (MeOH-POX). In fact, by using Eq. (7) it is possible to calculate the necessary flow rate of oxygen to bring the system outside the carbon formation region. For example, a SOFC fuelled directly with MeOH at 973 K is outside the carbon formation region if the fuel utilization is 13.25%. For POX operation, this condition must be achieved also at OCP (i.e. $I = 0$ A; $U_f = 0\%$). Therefore, it is necessary to artificially increase the fuel utilization (i.e. $U_{f\text{-}app} = 13.25\%$) by introducing air with the fuel. Assuming that air leaks are negligible (i.e. $n_{O_2-leaks} = 0\ \text{mol s}^{-1}$), from Eq. (7) the amount of O_2 to add with MeOH is $n_{O_2-POX} = U_{f\text{-}app} \times 0.25 \times z \times n_{fuel} = 0.198 \times n_{fuel}$, or $n_{air} = 0.964 n_{fuel}$, mol s^{-1}. The minimum O_2 to MeOH ratios for MeOH-POX as a function of the temperature are summarized in Table 2. The corresponding equilibrium compositions and potentials, as a function of the temperature, using the minimum amount of air required to avoid coking are shown in Fig. 2b.

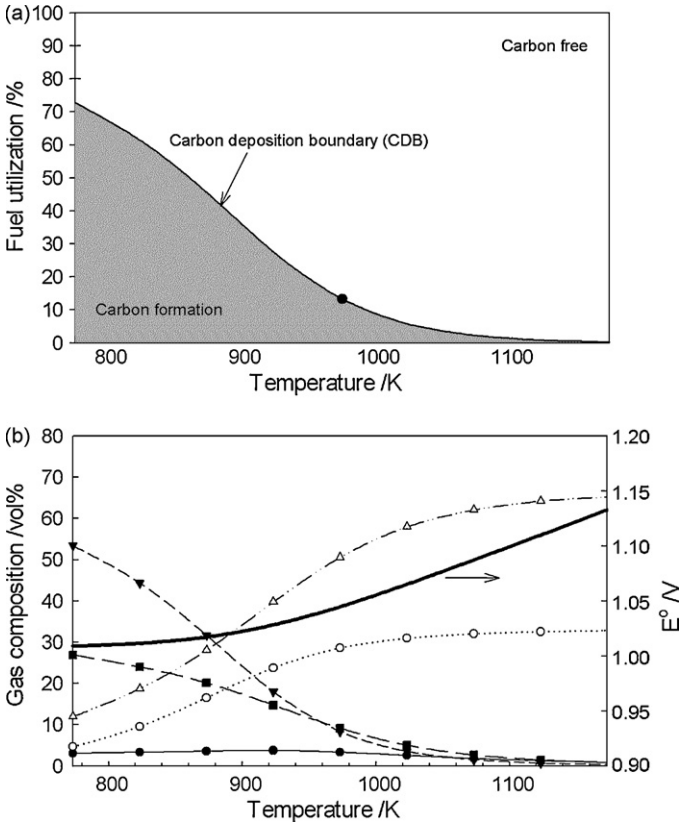

Fig. 2. Carbon formation region as a function of the temperature (a) for a SOFC fuelled with dry MeOH. Equilibrium composition potential (E^0) for the partial oxidation of MeOH (b) at the minimum air to fuel ratio to avoid coking. The species at equilibrium are (●) CH_4, (○) CO, (▼) CO_2, (△) H_2, and (■) H_2O.

Table 2
Minimum oxygen to fuel ratios (n_{O_2}/n_{fuel}) for MeOH and EtOH partial oxidation to avoid carbon formation.

T (K)	(n_{O_2}/n_{fuel})	
	MeOH	EtOH
773	1.1E+00	2.3E+00
823	9.2E−01	2.0E+00
873	6.8E−01	1.7E+00
923	4.1E−01	1.3E+00
973	2.0E−01	9.5E−01
1023	8.4E−02	7.2E−01
1073	3.3E−02	6.0E−01
1123	1.2E−02	5.4E−01
1173	3.4E−03	5.2E−01

Finally, the anode compositions and electromotive forces for the direct utilization of dry MeOH as a function of fuel utilization at three temperatures (1073, 973 and 873 K) were calculated (Fig. 3). These three graphs have some common features. As the fuel utilization increases the concentrations of H_2O and CO_2 increase, while the concentration of H_2 decreases. The concentration of CO increases with increasing fuel utilization within the carbon formation region, while it decreases when the fuel utilization is higher than the CDB. The H_2/CO does not change significantly with the fuel utilization. At 1073 K, the H_2/CO is approximately 2 even up to 80% fuel utilization. The EMFs at 0% fuel utilization (i.e. the equilibrium potential, E^0) are 1.084, 1.057, and 1.041 V at 1073, 973 and 873 K, respectively. As expected, the EMF decreases with increasing fuel utilization and the rate of this decrease is higher at higher temperatures. For example, at 1073 K the EMF decrease going from 0% to 80% fuel utilization is 0.181 V, while at 873 K the decrease is 0.088 V.

3.2. Equilibrium compositions with ethanol feed

The equilibrium composition for the pyrolysis of EtOH as a function of temperature is shown in Fig. 4. As for MeOH, the EtOH conversion at equilibrium is always 100%, and the only stable species are H_2, CO, CH_4, CO_2, H_2O, and C. Species such as acetaldehyde (CH_3CHO), acetic acid (CH_3COOH), ethylene (C_2H_4) and formaldehyde (HCHO) are not predicted, but are likely to be important intermediates in the actual process. Carbon deposition is predicted over the entire temperature range considered. The amount of carbon at equilibrium decreases with the temperature stabilizing to approximately 20 mol% above 1123 K, at which EtOH is entirely decomposed to H_2, CO and C. The ratio of these species is in accordance with the reaction $C_2H_5OH = 3H_2 + CO + C$, such that only this reaction is required to determine the equilibrium composition above 1123 K.

Table 3 contains the reforming factors, yields, and selectivities for ethanol steam- and dry-reforming at temperatures between 773 and 1173 K. For the steam-reforming of EtOH, the minimum value of the reforming factor that should be used to avoid carbon formation is 1.125 at 1073 K (i.e. 112.5 mol of H_2O per 100 mol of EtOH). As shown earlier, the minimum steam-reforming factor for MeOH is only 0.060 (20 times lower), which makes direct utilization almost indistinguishable from direct internal reforming in the case of methanol. A steam-reforming factor equal to 1.125 corresponds to an EtOH–H_2O liquid mixture containing 25.7 vol% H_2O, which is more than 5 times larger than in the azeotropic mixture and more than 3 times than in the typical commercial alcohol formulation. The reforming factor corresponding to the CDB decreases with temperature, and approaches 1 for temperatures above 1123 K in accordance with the stoichiometry of EtOH reform-

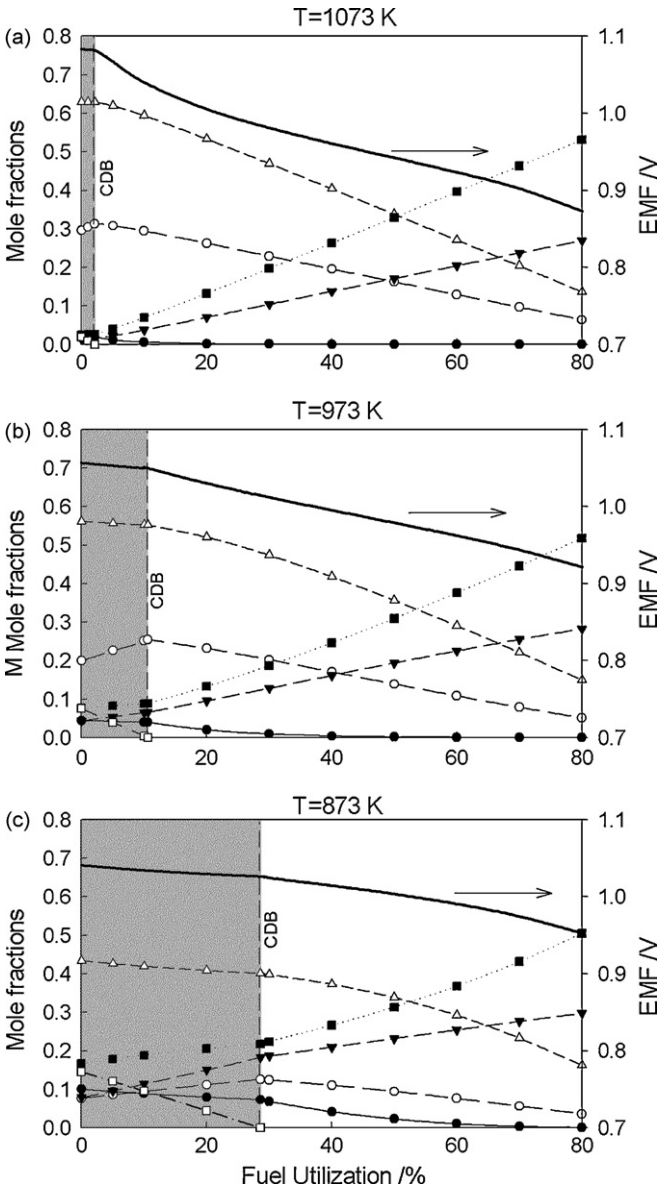

Fig. 3. Equilibrium composition and electromotive force for a SOFC operated with dry MeOH at (a) 1073 K, (b) 973 K, and (c) 873 K. The species at equilibrium are (●) CH_4, (○) CO, (▼) CO_2, (△) H_2, (■) H_2O, and (□) C (graphite).

Table 3
Minimum reforming factors required to avoid carbon formation in the steam- and dry- reforming of ethanol, and the resulting H_2 yield, CH_4 yield and H_2/CO ratios.

T (K)	EtOH steam-reforming				EtOH dry-reforming			
	RF_{H_2O}	Ey_{H_2}	Ey_{CH_4}	$ES_{H_2/CO}$	RF_{CO_2}	Ey_{H_2}	Ey_{CH_4}	$ES_{H_2/CO}$
773	2.709	1.660	1.051	12.232	81	0.756	0.014	0.146
823	2.670	2.314	0.841	7.209	33	1.075	0.028	0.224
873	2.416	2.898	0.617	4.568	14	1.449	0.050	0.333
923	2.051	3.341	0.407	3.244	6.25	1.846	0.072	0.478
973	1.583	3.530	0.267	2.519	3.2	2.210	0.074	0.633
1023	1.269	3.700	0.176	2.149	1.85	2.516	0.069	0.785
1073	1.125	3.787	0.100	2.090	1.35	2.712	0.053	0.882
1123	1.046	3.818	0.073	2.020	1.15	2.780	0.031	0.925
1173	1.014	3.869	0.050	2.002	1.07	2.893	0.027	0.964

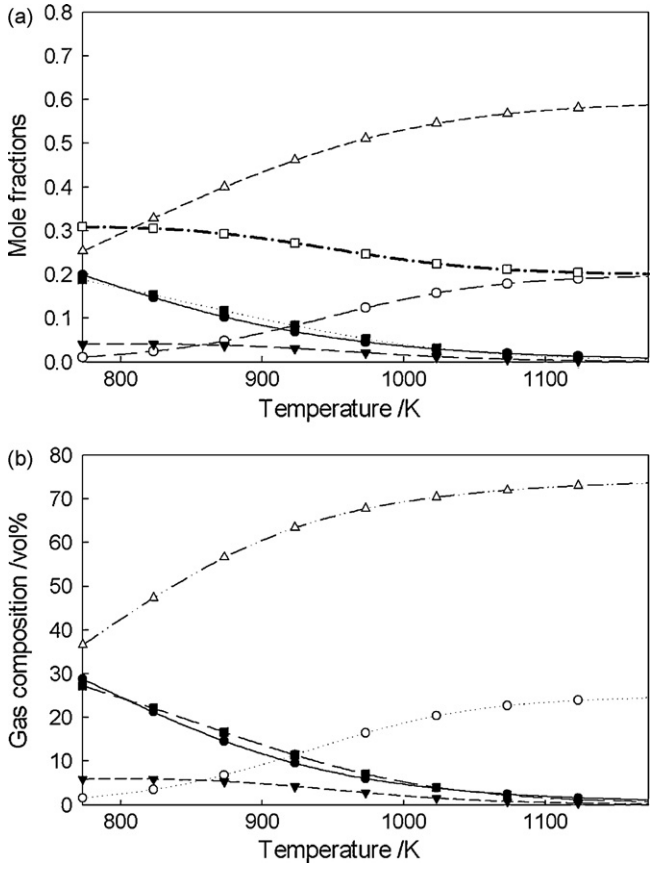

Fig. 4. Equilibrium composition (a) and gas-phase composition (b) as a function of the temperature for the reaction of EtOH pyrolysis. The species at equilibrium are (●) CH_4, (○) CO, (▼) CO_2, (△) H_2, (■) H_2O, and (□) C (graphite). Equilibrium composition potential (E^0) for the partial oxidation of EtOH (b) at the minimum air to fuel ratio to avoid coking. The species at equilibrium are (●) CH_4, (○) CO, (▼) CO_2, (△) H_2, and (■) H_2O.

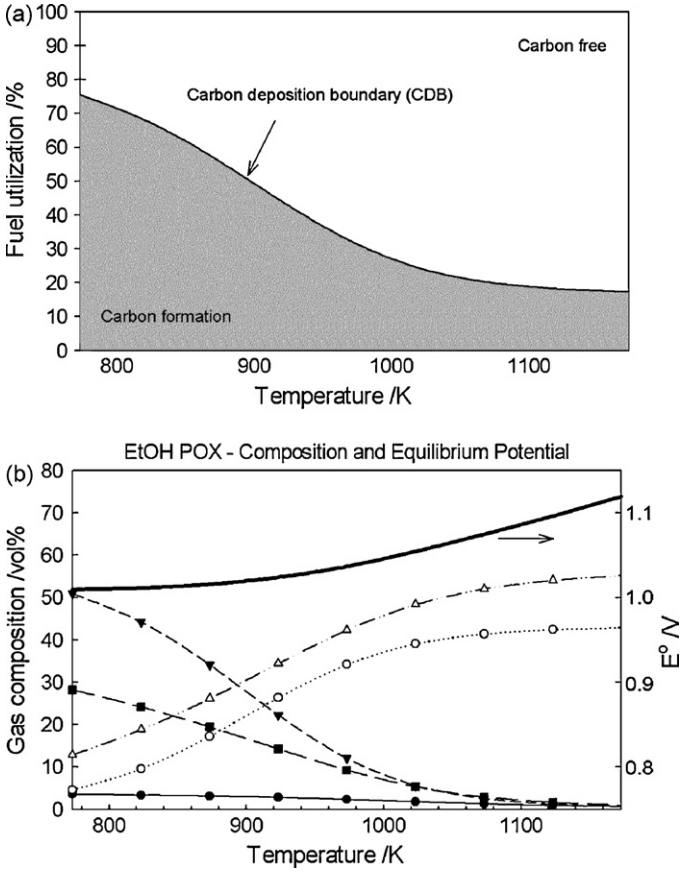

Fig. 5. Carbon formation region as a function of temperature for a SOFC fuelled with dry EtOH.

ing (i.e. $CH_3CH_2OH + H_2O = 4H_2 + 2CO$). Consistently, the yield of hydrogen (Ey_{H_2}) increases with temperature and approaches a value of 4, while the hydrogen to carbon monoxide ratio ($ES_{H_2/CO}$) decreases with temperature and approaches a value of 2. The quantity of CH_4 present at equilibrium decreases with temperature, consistent with the conversion to H_2 and CO being the dominant reaction.

As for MeOH, the dry-reforming of EtOH requires relatively high reforming factors to avoid carbon formation at temperatures lower than 973 K. Also in this case, the presence of CO_2 promotes carbon formation at 773 K for reforming factors smaller than 2 if compared to EtOH pyrolysis. The reforming ratio decreases with temperature and approaches 1 for temperatures higher than 1123 K as in the stoichiometry of the EtOH dry-reforming reaction (i.e. $CH_3CH_2OH + CO_2 = 3H_2 + 3CO$). Similarly, Ey_{H_2} increases with temperature approaching 3, while $ES_{H_2/CO}$ approaches 1. The equilibrium yield for CH_4 is always low relative to that for H_2 and CO and reaches a maximum at approximately 923 K.

Equilibrium compositions were calculated as a function of fuel utilization considering an inlet stream composed of dry EtOH and oxygen transported through the electrolyte in the proportions given by Eq. (5). From the results obtained, the region of carbon deposition was identified as shown in Fig. 5a. The required fuel utilization required to avoid carbon formation decreased with temperature. For example, at 973 K the minimum fuel utilization to avoid coking is 28.7%, while at 1073 K it is 19.5%. Unlike the case with MeOH, the CDB line does not approach zero at high temperatures (compare with Fig. 2). The equilibrium composition and potential, as a function of temperature, in the case of partial oxidation of ethanol (EtOH-POX) using the minimum amount of air required to avoid coking is shown in Fig. 5b. The minimum O_2 to fuel ratio for the POX of EtOH as a function of the temperature are summarized in Table 2. Because the extent of carbon formation is greater with EtOH than MeOH, the minimum levels of O_2 are between approximately 2 (at 773 K) and approximately 150 (at 1173 K) times larger for EtOH.

The equilibrium compositions and EMF for the direct utilization of EtOH as a function of fuel utilization at 1073, 973 and 873 K are shown in Fig. 6a–c, respectively. The trends of the stable species in Fig. 6 are similar to those seen for MeOH in Fig. 3. Specifically, with increasing fuel utilization the concentrations of H_2O and CO_2 increase, while the concentration of H_2 decreases. The concentration of CO initially increases, reaches a maximum at the CDB, and then decreases with fuel utilization. The H_2/CO ratio decreases for fuel utilizations greater than the CDB. The concentration of CH_4 decreases significantly with temperature. At 873 K, the maximum CH_4 concentration is 14.6 vol%, while at 1073 K the maximum concentration is 2.4 vol% (also see Fig. 4a). In both cases, these maxima occur at 0% fuel utilization. The EMFs at 0% fuel utilization are 1.103, 1.068, and 1.052 V at 1073, 973 and 873 K, respectively. The EMF decreases with increasing fuel utilization, decreasing approximately 0.225 V when going from 0% to 80% fuel utilization at 1073 K. As for MeOH, the change in EMF with fuel utilization decreases with decreasing temperatures.

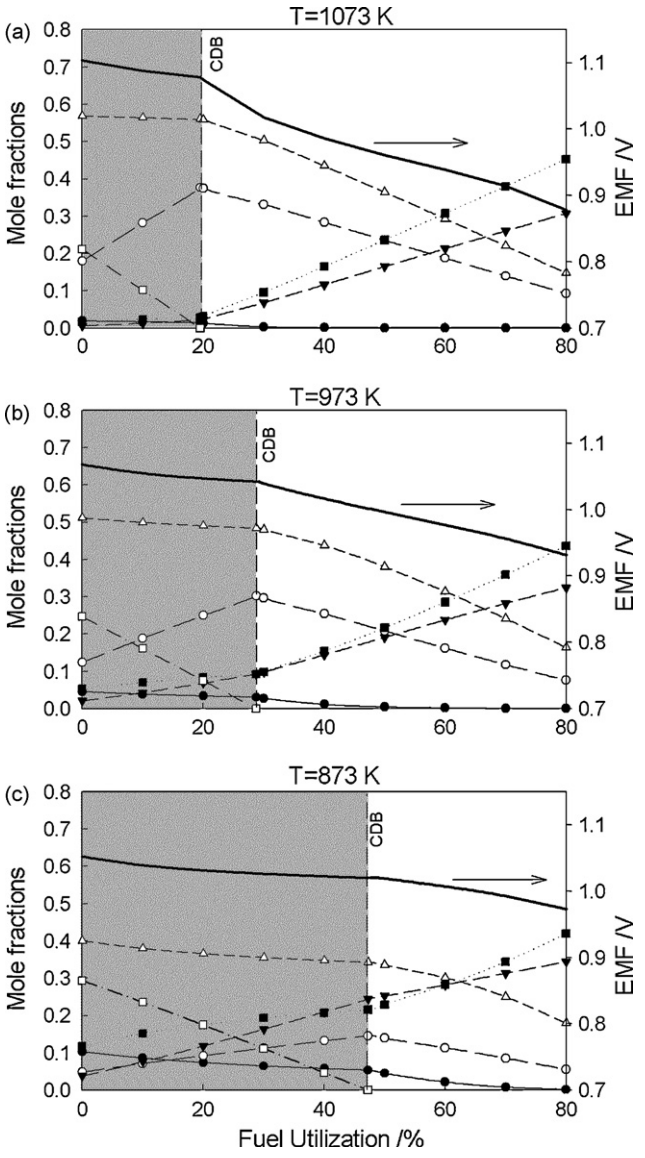

Fig. 6. Equilibrium composition and electromotive force for a SOFC operated with dry EtOH at (a) 1073 K, (b) 973 K, and (c) 873 K. The species at equilibrium are (●) CH_4, (○) CO, (▼) CO_2, (△) H_2, (■) H_2O, and (□) C (graphite).

3.3. Effect of using thermodynamic data for amorphous carbon

Several studies have shown that the type of carbon deposited in SOFC depends on the type of hydrocarbon used as fuel [2], on the anode material [25], and possibly also on other factors, such as aging and history of the sample [20]. Thermodynamic measurements indicate that graphite is more stable than amorphous carbon. Unfortunately, there are only a few studies reporting the enthalpy and entropy of formation for amorphous carbon [26–28], and there is no agreement on the enthalpy and entropy difference between amorphous carbon relative to graphite [29,30]. According to [28] the enthalpy of formation of amorphous carbon is 15.400 kJ mol^{-1} higher than that of graphite, while the entropy is 4.1 J K^{-1} mol^{-1} higher, compatible to the higher disorder of the amorphous structure. The standard Gibbs free energy for the transformation of amorphous carbon into graphite was found to be −11.054 kJ mol^{-1}. In another study [26], the enthalpy difference varied significantly depending on the degree of amorphousness of the carbon, but the standard Gibbs free energy for the transformation of amorphous carbon into graphite was in all cases smaller than −3.220 kJ mol^{-1}. The effect on the equilibrium composition of using thermodynamic data for amorphous carbon rather than graphite was investigated for the Boudard reaction ($2CO = C_{(s)} + CO_2$) and for the methane decomposition ($CH_4 = C_{(s)} + 2H_2$) using the thermodynamic data for amorphous carbon proposed in [28].

The equilibrium constant for the Boudard reaction calculated using the standard thermodynamic data at 773 K for graphite is 6.7 times higher than that obtained using the data for amorphous carbon, while at 1173 K the equilibrium constant is 2.9 times higher for graphite. The ratios of the equilibrium constant for the methane decomposition reaction vary in a similar fashion. Thus, the effect of using the values for amorphous carbon instead of the values for graphite, is a decrease of the moles of carbon ($C_{(s)}$) present at equilibrium for both MeOH and EtOH. If both graphite and amorphous carbon are included in the calculation of the equilibrium composition, the moles of amorphous carbon are negligible in all cases, and the resulting composition is identical to that obtained using only the data for graphite. This result was expected since the energy content of amorphous carbon is higher that graphite. In addition, it is expected that amorphous carbon should transform into graphite over time (i.e. aging), as this reaction is exothermic.

4. Conclusions

According to the results of the equilibrium calculations presented in this paper, H_2 and CO are the main products of MeOH pyrolysis. The presence of C is predicted over the temperature range considered but the equilibrium concentration decreases significantly with temperature, becoming less than 2 mol% above 1073 K. At these temperatures, the equilibrium constant for the reaction $CH_3OH = 2H_2 + CO$ is higher than any other decomposition pathway such that only this reaction needs to be considered to estimate the equilibrium composition. The presence of small quantities of H_2O in the (liquid) MeOH used to fuel the SOFC (e.g. 2.6 vol% for a SOFC operating at 1073 K) should be sufficient to suppress carbon formation at equilibrium; therefore, the purity of the feed is important in experimentation to ensure that the SOFC is operated in the direct utilization mode. Carbon formation also becomes thermodynamically unfavourable when the SOFC is producing current. The minimum values of fuel utilizations for which graphite is not present at equilibrium were identified. For MeOH, the fuel utilization value at the carbon formation boundary is 2.1% at 1073 K, and higher fuel utilizations are needed to operate in the carbon free region.

For EtOH pyrolysis, the main products at equilibrium are H_2, CO and C. The reaction $C_2H_5OH = 3H_2 + CO + C$ dominates the equilibrium of decomposition above 1123 K. For EtOH steam-reforming, relatively large amounts of H_2O must be added to pure EtOH in order to prevent carbon formation (e.g. 25.7 vol% for a SOFC operating at 1023 K). The carbon deposition boundary was calculated as a function of the fuel utilization. At 1073 K, the minimum fuel utilization for a SOFC fuelled with dehydrated EtOH to operate outside the carbon formation region is 19.5%.

The use of thermodynamic data for amorphous carbon rather than graphite in the calculation of the thermodynamic equilibrium results in a decrease in the amount of solid carbon present at equilibrium. Because the energy content of amorphous carbon is significantly higher than graphite, the use of both amorphous carbon and graphite in the calculations results in the same final equilibrium composition as using only graphite.

In an operating SOFC there might be significant deviations from equilibrium. One such deviation, for instance, is related to the incomplete conversion of the alcohols. However, the equilibrium conditions described in this paper are indicative of the final state towards which the system may evolve.

Acknowledgements

This work was financed with a Natural Sciences and Engineering Research Council (NSERC) grant. The authors are grateful to Dr. Pedro A. Pereira for the use of FactSage 5.4. M.C. is grateful to NSERC and Killam Trust for financial support.

References

[1] W. Vielstich, A. Lamm, H.E. Gasteiger, Handbook of Fuel Cells—Fundamentals Technology and Applications, 1st ed., John Wiley & Sons Ltd., West Sussex, 2003.
[2] S.C. Singhal, K.E. Kendall, High Temperature Solid Oxide Fuel Cells—Fundamentals, Design and Applications, 1st ed., Elsevier Ltd., Oxford, UK, 2003.
[3] Z. Zhan, J. Liu, S.A. Barnett, Applied Catalysis A: General 262 (2004) 255–259.
[4] M.D. Gross, J.M. Vohs, R.J. Gorte, Journal of Materials Chemistry 17 (2007) 3071–3077.
[5] G. McIntosh, Chemical Reviews 104 (2004) 4845–4865.
[6] T. Kim, G. Liu, M. Boaro, S.I. Lee, J.M. Vohs, R.J. Gorte, O.H. Al-Madhi, B.O. Dabbousi, Journal of Power Sources 155 (2006) 231.
[7] S.C. Singhal, Solid State Ionics 152 (2002) 405–410.
[8] G.A. Olah, Chemical & Engineering News 81 (2003) 5–15.
[9] M. Boudart, Kinetics of Chemical Processes, Butterworth-Heinemann, 1968, p. 50.
[10] K. Sasaki, K. Watanabe, K. Shiosaki, K. Susuki, Y. Teraoka, Journal of Electroceramics 13 (2004) 669–675.
[11] K. Sasaki, Y. Teraoka, Journal of The Electrochemical Society 150 (2003) A878–A884.
[12] K. Sasaki, Y. Teraoka, Journal of The Electrochemical Society 150 (2003) A885–A888.
[13] S. Assabumrungrat, N. Laosiripojana, V. Pavarajarn, W. Sangtongkitcharoen, A. Tangjitmatee, P. Praserthdam, Journal of Power Sources 139 (2005) 55.
[14] S. Assabumrungrat, V. Pavarajarn, S. Charojrochkul, N. Laosiripojana, Chemical Engineering Science 59 (2004) 6015–6020.
[15] N. Laosiripojana, S. Assabumrungrat, Journal of Power Sources 163 (2007) 943–951.
[16] P. Tsiakaras, A. Demin, Journal of Power Sources 102 (2001) 210–217.
[17] J.-H. Koh, B.-S. Kang, H.C. Lim, Y.-S. Yoo, Electrochemical and Solid-State Letters 4 (2001) A12–A15.
[18] H.A. Liebhafsky, E.J. Cairns, Fuel Cells and Fuel Batteries—A Guide to Their Research and Development, John Wiley & Sons, Inc., New York, 1968.
[19] E.J. Cairns, A.D. Tevebaugh, G.J. Holm, Journal of The Electrochemical Society 110 (1963) 1025.
[20] V. Alzate-Restrepo, J.M. Hill, Applied Catalysis A: General 342 (2008) 49.
[21] W.R. Smith, R.W. Missen, Chemical Reaction Equilibrium Analysis: Theory and Algorithms, John Wiley & Sons, New York, 1982.
[22] H.S. Fogler, Elements of Chemical Reaction Engineering, 3rd ed., Prentice-Hall, Upper Saddle River, NJ, 1999.
[23] DIPPR® Project 801—Full Version, Evaluated Standard Thermophysical Property Values American Institute of Chemical Engineers, Provo, UT 84602, 2005.
[24] M. Cimenti, Direct utilization of methanol and ethanol in SOFC, PhD Thesis, University of Calgary, Calgary, Canada, 2008.
[25] S. McIntosh, H.P. He, S.I. Lee, O. Costa-Nunes, V.V. Krishnan, J.M. Vohs, R.J. Gorte, Journal of The Electrochemical Society 151 (2004) A604–A608.
[26] B.S. Terry, X. Yu, Ironmaking and Steelmaking 18 (1991) 27–32.
[27] J. Rostrup Neilsen, Journal of Catalysis 27 (1972) 343–356.
[28] K.T. Jacob, S. Seetharaman, Metallurgical and Material Transactions B 25B (1995) 149–151.
[29] K.T. Jacob, S. Seetharaman, Metallurgical and Material Transactions B 25B (1995) 656–658.
[30] B.S. Terry, X. Yu, Metallurgical and Material Transactions B 25B (1995) 655–656.